Cold Regions Science and Technology 179 (2020) 103139

Contents lists available at ScienceDirect

Cold Regions Science and Technology

journal homepage: www.elsevier.com/locate/coldregions

Effects of the ICE-T microphysics scheme in HARMONIE-AROME on estimated ice loads on transmission lines

Bjørg Jenny Kokkvoll Engdahl[a,b,*], Bjørn Egil Kringlebotn Nygaard[c], Vemund Losnedal[d], Gregory Thompson[e], Lisa Bengtsson[f,g]

[a] Norwegian Meteorological Institute, Henrik Mohns plass 1, 0371 Oslo, Norway
[b] Department of Geosciences, University of Oslo, Sem Sælands vei 1, 0371 Oslo, Norway
[c] Norconsult AS, Tærudgata 16, 2004 Lillestrøm, Norway
[d] Norwegian University of Life Sciences, Universitetstunet 3, 1430 Ås, Norway
[e] National Center for Atmospheric Research, P.O. Box 3000, Boulder, CO, USA
[f] National Oceanic and Atmospheric Association, Earth System Research Laboratory (NOAA-ESRL), 325 Broadway, 80303-3328 Boulder, CO, USA
[g] Cooperative Institute for Research in Environmental Sciences (CIRES), University of Colorado, Boulder, CO, USA

ARTICLE INFO

Keywords:
In-cloud icing
Ice accretion on transmission lines
Numerical modelling
Cloud microphysics
Weather forecast

ABSTRACT

In-cloud icing can cause damage to infrastructure and is challenging to forecast due to lack of a good representation of supercooled liquid water (SLW) in numerical weather prediction (NWP) models. We validate the new microphysics scheme, ICE-T, implemented into the NWP model HARMONIE-AROME, in full 3D simulations running over a 3 month period from December 1st 2016 to February 28th 2017. Output from the model simulations are first compared with conventional observations to evaluate the overall quality, and then used as input to an ice accretion model (IAM) and compared against measured ice loads at the two test sites Hardingnuten and Ålvikfjellet. The results show a clear shift towards more cloud water and snow, and less graupel and cloud ice. This shift leads to less precipitation along the coast and more inland. The estimated ice loads based on the cloud water from the simulations are generally increased. We also focus on two different icing events during January 9–18 and February 1–14. During the first event, both the run in its original configuration and the run with ICE-T overestimated the ice loads, while the second event was underestimated. For Ålvikfjellet ICE-T gives the best estimates, while for Hardingnuten the ice loads are overestimated when the wind direction is from the southeast. This is due to local terrain shielding not captured by the model. During the Feb 1–14 event, the wind direction was generally easterly, which makes comparison between the simulations and the observations more reliable. In this case, ICE-T gives a better ice load estimate. Although there are major uncertainties, especially concerning the number concentration of cloud droplets, and local terrain effects, ICE-T appears to give a better estimate of the ice loads.

1. Introduction

Atmospheric icing occurs when supercooled liquid water (SLW) droplets freeze upon objects that it comes in contact with (Belo-Pereira, 2015). This can cause severe problems for road and air traffic (Kalinka et al., 2017), lead to production loss and mechanical malfunctioning on wind turbines (Hämäläinen and Niemelä, 2017), and bring down transmission lines and other infrastructure (Farzaneh, 2008). Hilly areas in mid- to high latitude countries are often exposed to atmospheric icing from orographic lifting. In these locations reliable estimates of the expected ice loads on infrastructure is of utmost importance. During the winter of 2013–2014 two major transmission lines in the western mountain regions of Norway suffered severe damage due to atmospheric icing. The ice loads accreted upon one of the lines were measured to be 68 kg/m (Fig. 1), which is more than twice the design load of the line (Nygaard et al., 2017). To avoid similar scenarios in the future, accurate estimates of ice loads are needed, however, the estimation of build-up of ice on surfaces is a complex task as it depends on physical processes - and their interaction - on atmospheric scales ranging from in-cloud microphysics to synoptic scale wind patterns.

A common method to estimate ice loads is to use meteorological output from numerical weather prediction (NWP) models (Harstveit et al., 2009). However, a known deficiency of the in-cloud microphysics schemes in many NWP models is the representation of SLW - critical for

* Corresponding author at: Norwegian Meteorological Institute, Henrik Mohns plass 1, 0371 Oslo, Norway.
E-mail address: bjorgjke@met.no (B.J.K. Engdahl).

https://doi.org/10.1016/j.coldregions.2020.103139
Received 3 January 2020; Received in revised form 8 July 2020; Accepted 20 July 2020
Available online 24 July 2020

Fig. 1. Collapsed transmission line at Ålvikfjellet in January 2014. The ice loads were measured to 68 kg/m. Photo: Ole Gustav Berg, Statnett.

atmospheric icing processes - as they often tend to produce ice at the expense of liquid water once the temperature drops below 0 °C (Nygaard et al., 2011). In this study we seek to improve the representation of SLW in the NWP model generating the meteorological data used for the ice-load estimations. The aim is to improve the forecasts of atmospheric icing on infrastructure, and future estimates of maximum ice loads.

The NWP model used in this study is the HARMONIE-AROME model (Bengtsson et al., 2017; Seity et al., 2011; Brousseau et al., 2016) which is used operationally at MET-Norway and 10 other European countries. Similar to many other NWP models it suffers from over-estimating in-cloud ice at the expense of SLW (e.g. Hämäläinen and Niemelä, 2017; Bengtsson et al., 2017). Engdahl et al., 2020 (hereafter ENG20) tested the HARMONIE-AROME model's ability to represent SLW, and created two idealised test cases for atmospheric icing, one orographic lift case and one freezing drizzle case, using the 1D column version of HARMONIE-AROME called MUSC. They showed that the HARMONIE-AROME model had a tendency towards more ice species and less SLW for both cases. In order to improve the representation of SLW, ENG20 implemented elements from the Thompson et al., (Thompson et al., 2004; Thompson et al., 2008) microphysics scheme into HARMONIE-AROME. Their final iteration of the microphysics code showed a clear increase and a prolonged existence of SLW, compared with the original code in both idealised cases.

The current study is a continuation of ENG20, where we now move away from the idealised test environment and into full scale 3D-simulations with real cases. Specifically, we want to test the modified microphysics scheme's ability to forecast icing events on transmission lines using specialised observations of ice loads. The meteorological output from both the original scheme (CTRL) and the modified scheme (ICE-T) are fed into an ice accretion model (IAM) and the resulting ice-loads are compared with the observations. Long term statistics are generated over a period that includes several well documented icing events both at Hardingnuten and Ålvikfjellet test-sites. The two sites are located on either side of the central mountains in Southern-Norway (Fig. 2), which means that they normally do not experience icing at both locations simultaneously, and therefore represent different icing climatologies.

In addition to the long term icing statistics, we also dive into two cases, one where we found our ice-load estimates to be underestimated, and one where the ice loads were overestimated in our simulations. We seek to understand how different factors impact both the simulated and observed ice loads, and how the uncertainties can be reduced in the future.

Finally, since the microphysics scheme in an NWP model not only affects SLW (Liu et al., 2011), we also compare the differences in precipitation amounts and patterns, hydrometeor distributions, and cloud cover. Changes in precipitation and cloud cover can also impact downstream meteorological parameters such as temperatures, pressure fields, and wind speeds. For an operational NWP model, it is important that the quality of these downstream parameters are not significantly worsened. Therefore, we also do general verification of the simulations against MET-Norway's grid of conventional observations.

The main goal of the present study is to develop a new microphysics scheme with a more accurate representation of SLW, that can be used both for operational forecasting for aviation and of ice accretion on structures, downscaling of climate projections for future icing climatologies, as well as general forecast to the public.

2. Methodology

2.1. The HARMONIE-AROME NWP model

HARMONIE-AROME is a non-hydrostatic convection permitting NWP model based on the AROME model developed at Meteo-France (Seity et al., 2011; Brousseau et al., 2016). It is developed and maintained by the international consortia for developing regional weather models in Europe called Hirlam-Aladin (Termonia et al., 2018; Bengtsson et al., 2017). It has been the basis for the operational weather forecast at MET-Norway since 2014 (Müller et al., 2017), and is widely used for operational weather forecasts by national weather service centres in Europe. HARMONIE-AROME is also used for climate downscaling, where an accurate representation of in-cloud ice and liquid water is of high importance for climate feedback (Tan et al., 2016). The model physics used in HARMONIE-AROME is outlined in detail in Bengtsson et al. (2017), below we summarize some of the main components.

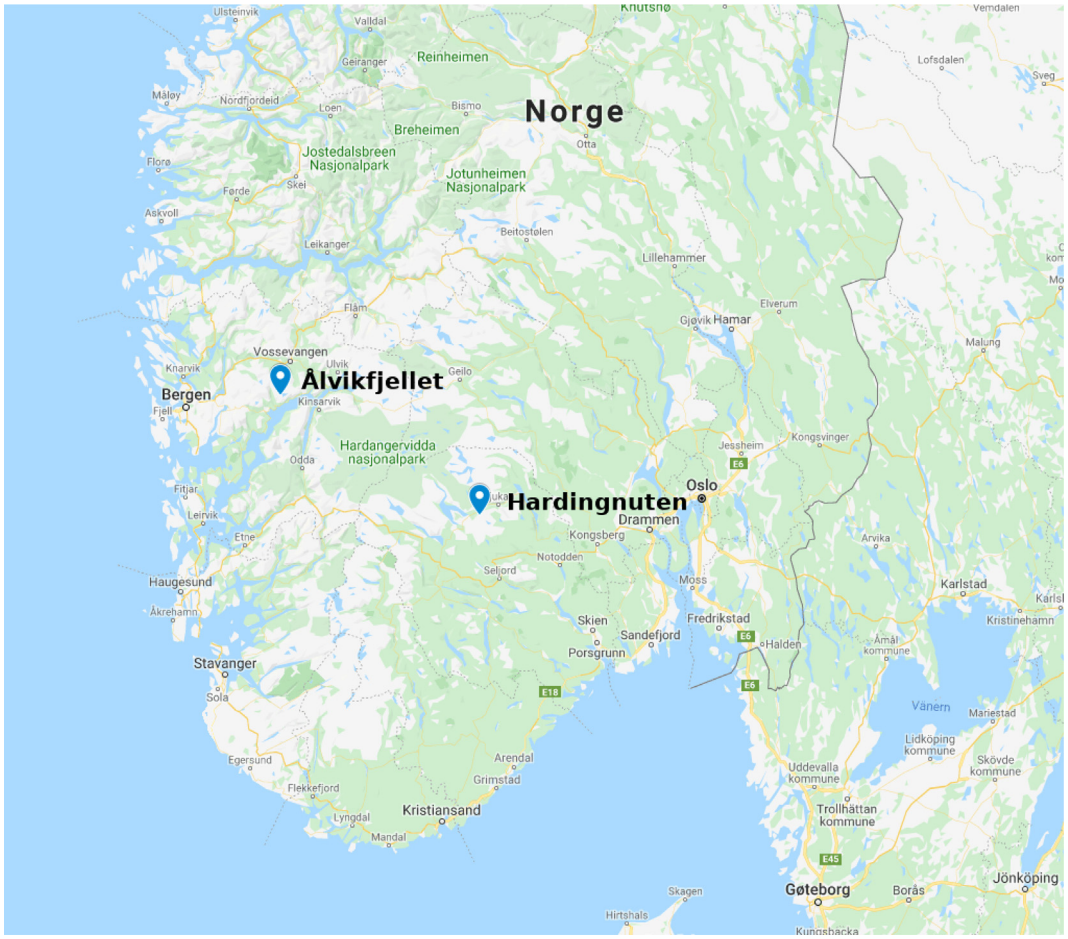

Fig. 2. Map of southern Norway with the location of Hardingnuten and Ålvikfjellet observation sites. Created with google maps.

The mixing by turbulent eddies and convective plumes in HARMONIE-AROME is done using a so called Eddy Diffusion Mass Flux (EDMF) scheme, where the eddy diffusion mixing uses a prognostic equation for the turbulent kinetic energy (TKE) combined with a diagnostic mixing length scale (Lenderink and Holtslag, 2004). Deep cumulus convection is assumed to be resolved by the dynamics (using a horizontal grid-distance of 2.5 km), however there is still a sub-grid representation of the mass-flux mixing by shallow convection. This parameterization consists of a dual mass-flux framework in which both a dry and a moist updraft is represented and follows the methodology outlined in Neggers et al. (2009).

The cloud microphysics scheme in HARMONIE-AROME is called ICE3 and is mostly based on Cohard and Pinty (2000a,b), with physics that can be traced back to Lin et al. (1983), Rutledge and Hobbs (1984), and Ferrier (1994). ICE3 is a single-moment bulk microphysics scheme, with prognostic calculations of the mass of cloud water, rain, cloud ice, snow, and graupel. In 2014, changes to the original scheme were implemented in order to improve the representation of SLW, in particular with respect to improve the forecasts of fog, low level clouds and cirrus clouds (Müller et al., 2017), all of which were related to too much ice - this update was referred to as “OCND2”.

In ENG20 idealised experiments using ICE3 with the changes implemented in OCND2 were carried out. It was found that the microphysics still had a tendency to quickly deplete the SLW. In short, cloud ice was introduced immediately when ice supersaturation was reached, which lead to an excess production of snow and graupel at the expense of SLW. To allow SLW to persist, several changes to ICE3/OCND2 were introduced in ENG20 based on Thompson et al. (2004, 2008). These changes consist of autoconversion, rain accreting cloud water, ice initiation, snow and graupel collecting cloud droplets and rain, mass-diameter relation and fall speed, and rain size distribution. Of these, the changes to the ice initiation (stricter conditions), snow and graupel collection of cloud droplets (less efficient collection), and rain size distribution (allow smaller rain drops for drizzle), had the most impact. An overview of the differences between the two schemes is found in Table 1 in ENG20. In their final version of the microphysics scheme, ENG20 showed that the SLW mixing ratio had doubled in both of the idealised cases, and had prolonged existence.

2.2. Experimental setup

In this study we compare the final modified microphysics scheme presented in ENG20 - here called ICE-T - with the default microphysics scheme in HARMONIE-AROME (version 40 h1.1), including the bug fix introduced in ENG20 (CTRL). The model domain is shown in Fig. 6, it consists of 949 × 739 grid points with Oslo in the centre, covering Norway, Sweden and parts of Finland. The horizontal grid-spacing is 2.5 km and there are 65 levels in the vertical. The domain is placed further west than the operational domain used by MEPS (Frogner et al., 2019), to allow for spin-up of the weather systems coming from the west. For these simulations, operational European Centre for Medium range Weather Forecasts (ECMWF) Integrated Forecast System (IFS) forecasts are used both on the lateral boundaries and as initial conditions every cycle, there is thus no upper air or surface data assimilation in these runs, nor initialisation of clouds or precipitation at the start of the simulations. Each cycle starts at 00 UTC and runs for 36 h. In the analysis we generally use +13 to 36 h, unless stated otherwise, this is to allow for some spinup of the atmospheric moisture and clouds and

precipitation, that our preliminary test runs have found to be 6 or more hours. The test period stretches from Dec 1 2016 to Feb 28 2017. CTRL is compared with the experiment consisting of the final version of the modified microphysics scheme found in ENG20.

The MET-Norway operational set up is described in Müller et al., 2017. The main differences between the operational setup and our experiments are cycling using data-assimilation of surface and upper air. New cycles are started every 3 h and an ensemble prediction system (EPS) of 11 members are generated. The boundary files are from the operational ECMWF-IFS data, with a delay of 3 and 6 h.

2.3. Ice accretion model (IAM)

To calculate the ice loads, we extracted the cloud water, specific humidity, and rain mixing ratios from the NWP model simulation output and utilised the time dependent IAM used in ISO12494 'Atmospheric Icing on Structures' and described in Makkonen (2000). This model also takes in wind speed and temperature to calculate the ice loads. A simple bias correction based on the observed wind speed was applied to the modelled wind speed, before the calculations were made. The observed temperature at each site was used as input to the IAM, so that the main difference between the calculated ice loads for CTRL and ICE-T stems from the modelled supercooled liquid water. In order to validate the time evolution of the ice loads, the IAM also includes routines to account for ice melting as well as ice sublimation. The sublimation routine calculates the ice loss based on basic thermodynamics when the ice saturation is less than 90%.

Furthermore, the IAM includes a calculation of the collision efficiency for the droplets to collide with the structure. This depends on the median volume droplet (MVD) size, as larger droplets have a higher probability to collide compared to smaller ones. MVD is calculated using the mass mixing ratio of SLW and the droplet number concentration, Nd. Higher Nd leads to smaller droplets, and lower ice accretion rates.

Nd is affected by several processes, like the background aerosol concentration, but also the evaporation and condensation processes. If an air parcel is lifted up a hill and then forced downwards on the other side, the smaller droplets can evaporate, while the larger can grow, leading to a shift in the size-distribution that a single-moment microphysics scheme can not account for. And since we do not have measurements of Nd on site, we ran the IAM with a range of Nd's (50, 100, 150 particles/cm^3) to span an interval of the uncertainty. We discuss the implications of this sensitivity in the results section. Hämäläinen and Niemelä (2017) stressed the importance and uncertainty of Nd, and chose a range of Nds (70, 100, 130, 300 particles/cm^3) to span the uncertainty over Finland. Since we only look at mountain stations with relatively clean air, a maximum of 150 particles/cm^3 was deemed appropriate.

The closest model grid-points to both of the sites had heights significantly lower than their actual heights (see Fig. 4). This could potentially lead to large errors, as the amount of cloud water is strongly dependent on the height. For Ålvikfjellet we used a nearby grid point with a more accurate height. Since the measurement site at Ålvikfjellet is situated at an exposed platou, there are not much terrain to shield any nearby point from icing, therefore a nearby point will experience the same icing conditions. However, this is not the case for the Hardingnuten measurement site. This site lies in the lee of a mountain top to the southeast, and is shielded to some extent from icing from this direction. Using a nearby grid-point with a more representable height, would thus not necessarily experience the same shielding effect. Therefore, for the Hardingnuten site, we used the data from the nearest grid-point, and then performed a height correction, where the air parcel is lifted to the exact height and the excess moisture is condensated and added to the cloud-water, whereas the specific humidity is likewise updated to maintain the water budget.

Fig. 3 shows the nearby terrain of both sites. Fig. 3a) includes transects in both southerly and north-easterly directions. The model and actual terrain height of both transects is shown in Fig. 4. From transect 1 (Fig. 4a) it is clear that the model terrain misses a mountain top of approximately 1400 m.a.s.l. around 7.5 km south of the measurement site. This top shields the measurement site from icing conditions coming from south.

In the north-easterly direction from the site (Fig. 4b), there is a narrow valley (between 3 and 4 km wide) that is not resolved in the model. For instance the town Rjukan, loacted inside the valley has an elevation of approximately 300 m.a.s.l., while the closest 9 model grid points ranges between 840 and 1242 m.a.s.l. in comparison. When the wind is easterly, the air will experience a steep lift from the valley up to the mountain where the measurement site is located. This effect will be underestimated in the simulations, as will be discussed in the results section.

3. Observation sites

3.1. Hardingnuten

The Hardingnuten observation site is located at 1229 m.a.s.l. near Rjukan in southern Norway (Fig. 2 and Fig. 3). Two transmission lines of 300 kV and 420 kV run in parallel close by, and atmospheric icing is frequently observed at these lines. The site measurements consist of an icing reference object (ISO12494) (IceTroll icing sensor), a heated 2D wind sensor and a temperature sensor. In addition, the Norwegian transmission system operator, Statnett, has installed load cells in suspension towers of the passing power lines, in order to measure in real time the ice load on the power line conductors. For this study we will focus on the IceTroll measurements.

There is also a disdrometer mounted on the observation mast at Hardingnuten. The disdrometer 'Thies LPM' (laser precipitation monitor) delivered by Adolf Thies & Co.KG is an instrument for measuring drop size from 0.125 mm and upwards, and velocity distribution of falling hydrometeors. The disdrometer consists of a transmitting laser diode that emits an infrared light-beam to a receiving photo diode which is transforming the optical intensity to an electrical signal. When a precipitation particle falls through the light beam the receiving signal is disturbed, and the electrical signal reduced. The particles size and velocity are determined by the amplitude and duration of the signal disturbance, respectively. The calculation comprises, among others, a particle spectrum, which is the distribution of the particles over a class binning containing 22 diameter classes and 20 velocity classes. The particle intensity is best visualized as a distribution matrix, with the velocity and particle diameter on the y- and x-axis, respectively. Further, by well-known empirical relationships between particle diameter and velocity of falling particles for different precipitation, one can classify the precipitation particle as e.g. water droplets (Atlas and Ulbrich, 1977), graupel (Locatelli and Hobbs, 1974), rime (Ishizaka, 1995), or snow. Hence, for a setup as the current on Hardingnuten, a qualitative classification of the hydrometeors is considered the most accurate.

3.2. Ålvikfjellet

Ålvikfjellet is located in Hardanger in the western part of Norway (Fig. 2 and Fig. 3b)). The test site lies on a plateou at 1086 m.a.s.l. and is highly exposed to icing due to lack of shielding, especially from southwesterly winds that bring moisture rich maritime air along the fjord and up the steep slope of the mountain (Ingvaldsen et al., 2019). A transmission line runs close by, where in 2014 ice loads of as much as 68 kg/m were detected. The measurements consist of a load cell installed on a test span in parallel with the transmission lines. There are also measurements of wind and temperature.

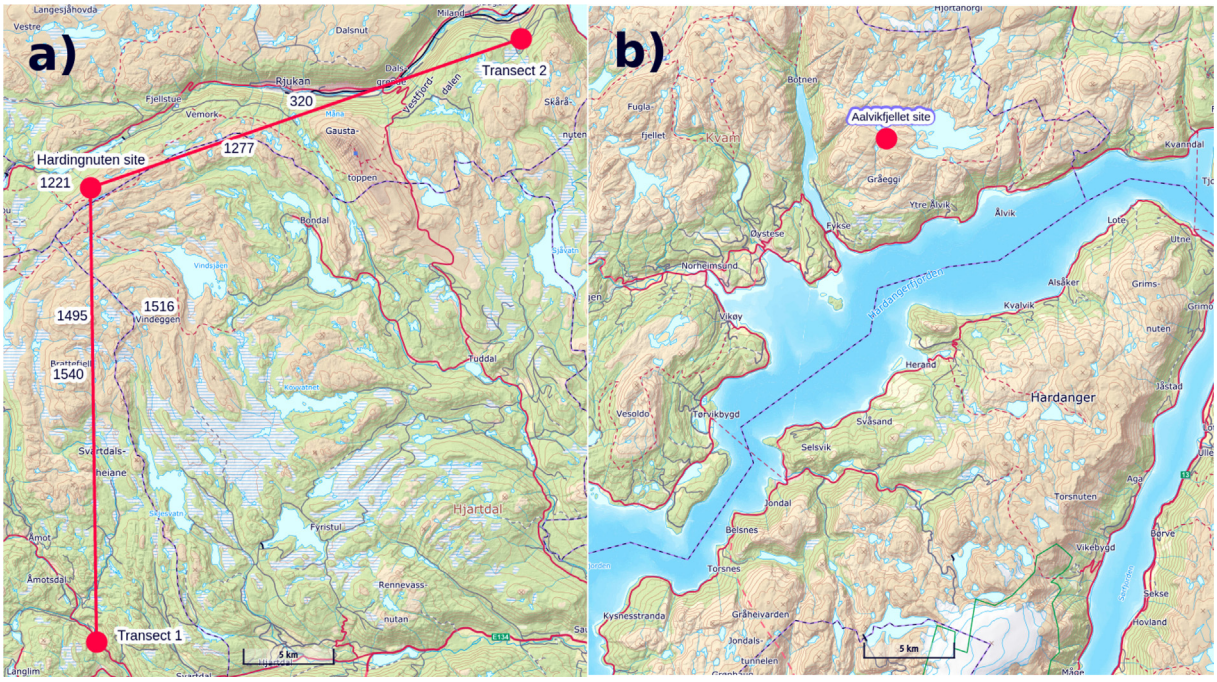

Fig. 3. Local terrain near Hardingnuten measurement site (a) and Ålvikfjellet measurement site (b). The red lines in the left panel shows the 25 km transects in Fig. 4. Figures made from norgeskart.no.

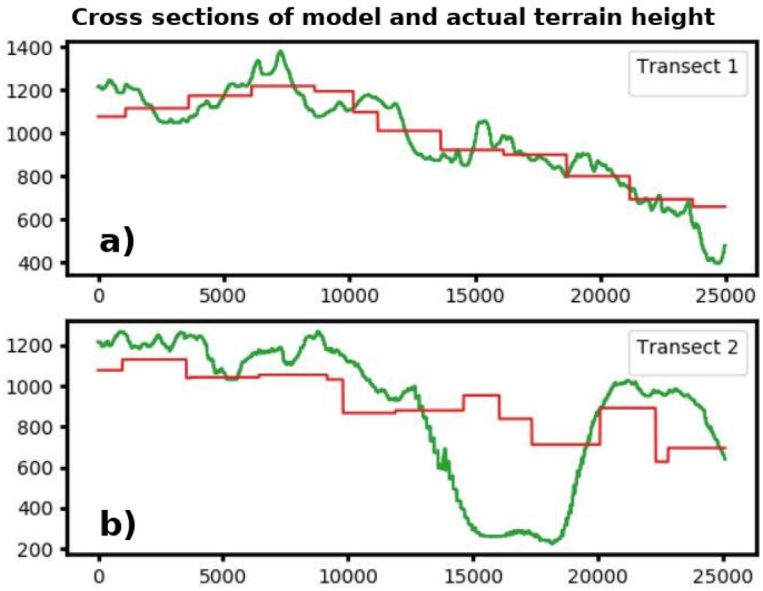

Fig. 4. Cross sections showing the model surface height (red lines) and actual height (green lines) along the transects depicted in Fig. 3a). Hardingnuten measurement site is located at the leftmost point in both transects. Actual terrain height taken from kartverket.no at 25 m resolution.

4. Results

4.1. General verification

We first verify that the general behaviour of the weather forecasts are not degraded by our updated cloud microphysics scheme. This is done by verifying against 177 conventional world meteorological organization (WMO) observation sites on the Norwegian mainland for the entire 3 months simulation, comparing control (CTRL) to the experiment (ICE-T) as well as to MET-Norway's operational weather forecasts (OPR) for the verification period. The verification of mean sea level pressure (MSLP), 2 m temperature (T2), 10 m wind speed (FF) and hourly precipitation (RR1) are presented in Fig. 5. It can be seen that the overall meteorology is not largely affected by the changes in microphysics. Furthermore, neither the ICE-T or CTRL runs show large errors compared with the operational forecasts for the time-period. For MSLP the verification scores are even better in the ICE-T and CTRL runs compared with the operational run, however, this is most likely due to the use of operational ECMWF analysis data on the lateral boundaries used in the ICE-T and CTRL simulations, compared with the MET-Norway operational simulation using 6 h old data.

There is a warm bias in the 2 m temperature for both the CTRL and ICE-T runs, which is likely due to the lack of surface data assimilation. In addition, the snow cover is based on input fields from ECMWF, which has a coarser resolution than the operational input fields. However, the 177 stations contain many near coastal stations, where the snow cover

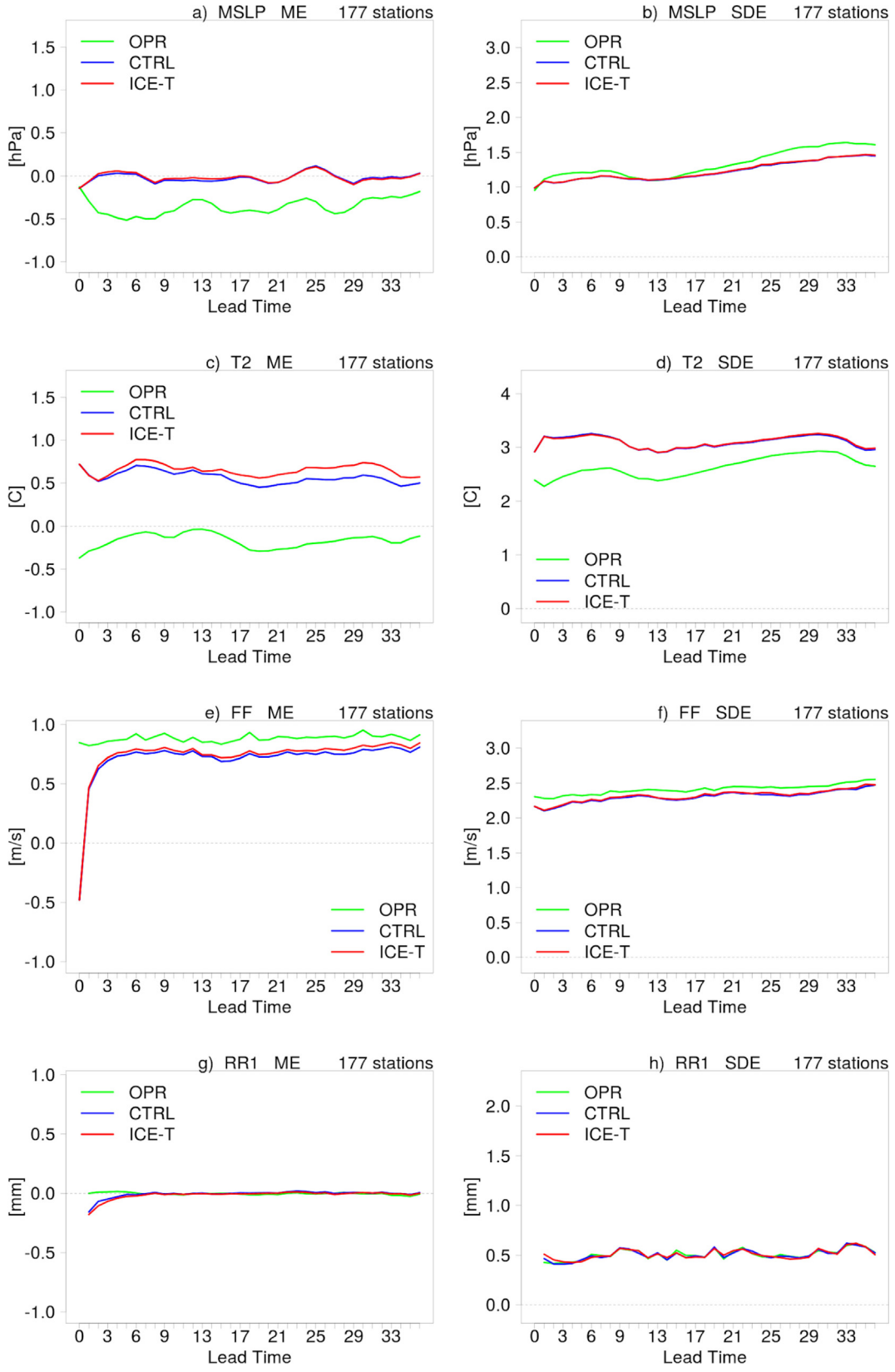

Fig. 5. Verification scores for CTRL and ICE-T. Mean error (ME) and standard deviation of error (SDE) for mean sea level pressure (MSL) (a) and b)), 2 m temperature (T2) (c) and d)), 10 min wind speed (FF) (e) and f)), and hourly precipitation (RR1) (g) and h)).

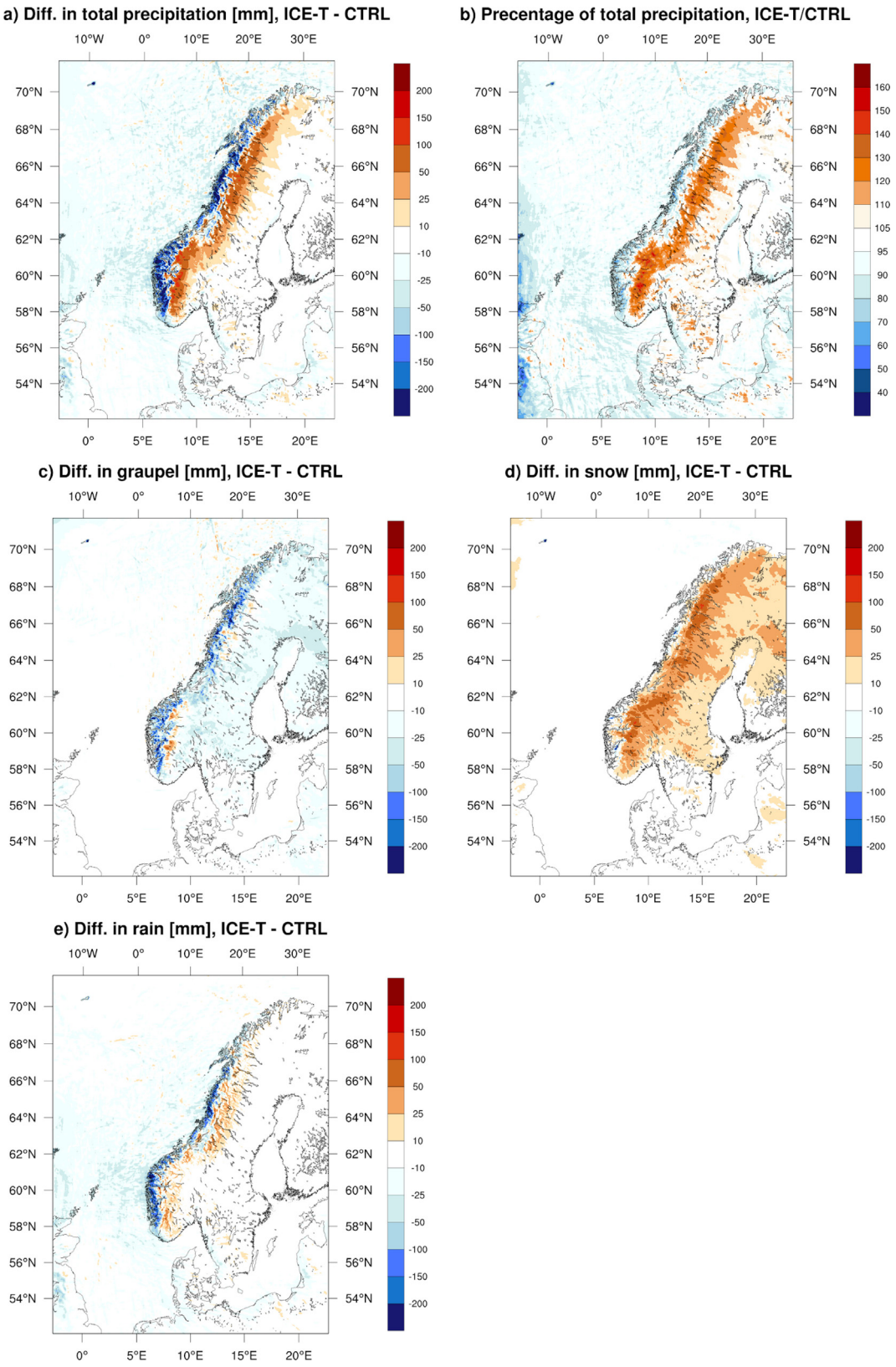

Fig. 6. Difference (ICE-T - CTRL) in precipitation for a) total precipitation, b) percentage of total precipitation (ICE-T/CTRL), c) graupel, d) snow, and e) rain.

will vary significantly over the winter, while in the mountain regions we focus on, the snow cover will be quite constant, therefore the input fields from ECMWF appear to be sufficient.

There were no large differences in the general cloud cover (not shown). This might seem a bit unexpected with large modifications to the cloud microphysics scheme, however the general cloud cover is mostly governed by large scale dynamics and terrain, which the microphysics have little impact on. The total cloud cover does not change much from CTRL to ICE-T. However, separating the low, middle, and high level clouds (not shown), reveal an increase in the low and middle

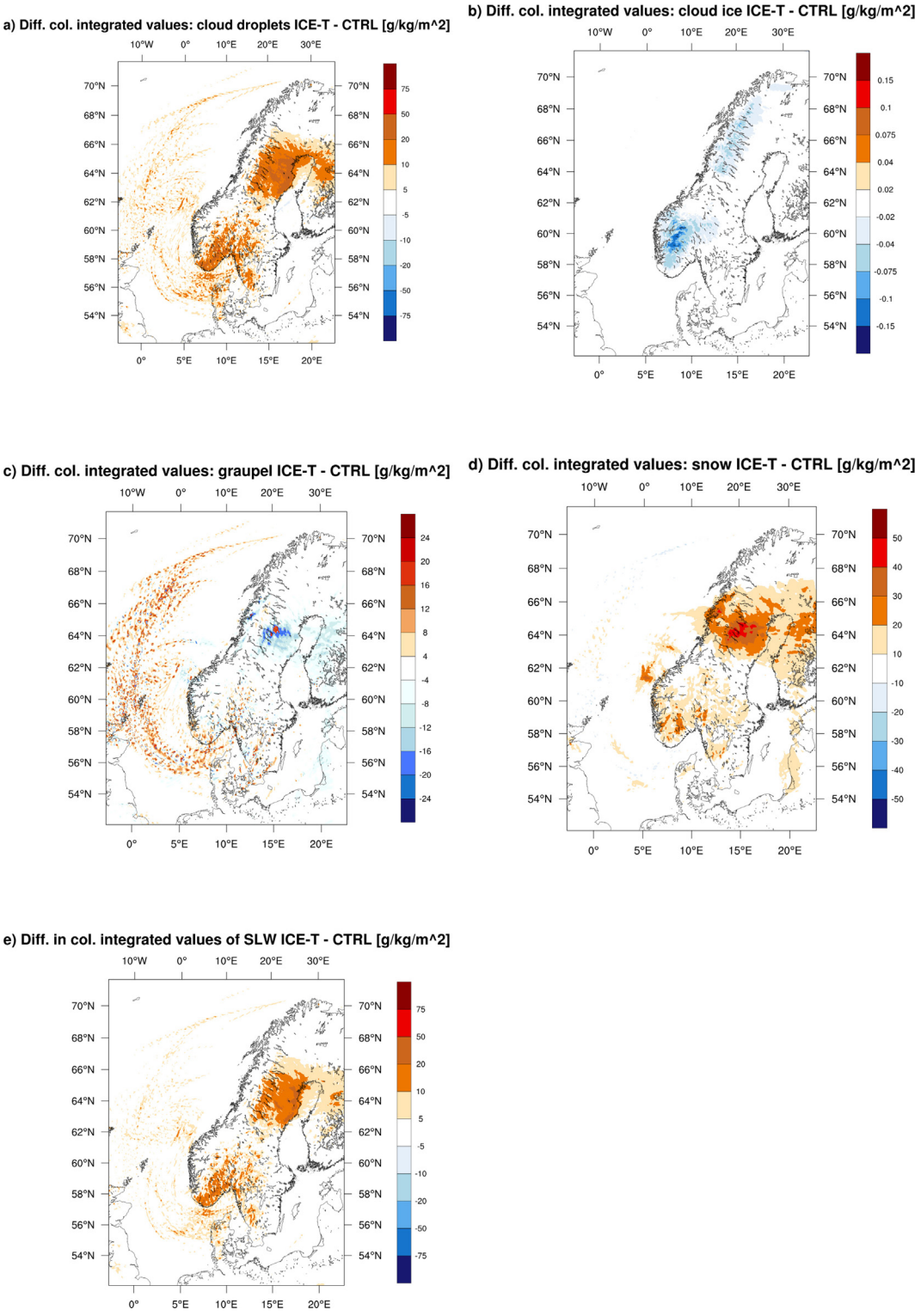

Fig. 7. Difference (ICE-T - CTRL) in column integrated values for the 35 lowest model levels of a) cloud water, b) cloud ice, c) graupel, d) snow, and e) supercooled liquid water.

level clouds, and a slight decrease in high level clouds, from CTRL to ICE-T. The decrease in high level clouds is seen only during the first few hours, and likely stems from the Meyers et al., 1992 ice nucleation as this only requires ice supersaturation to generate new ice, as discussed in ENG20. However, these hours are removed in the rest of the analysis to account for the spin-up time. For the middle and lower cloud fractions, the effect is larger and more persistent. The cloud fraction of lower clouds is increased by 10% and middle clouds by 15%. This increase is expected as water clouds tend to last longer than ice clouds.

4.2. Precipitation

Total accumulated precipitation (00UTC +13-36 h) over the entire domain shows that ICE-T has 95% of the total precipitation of CTRL.

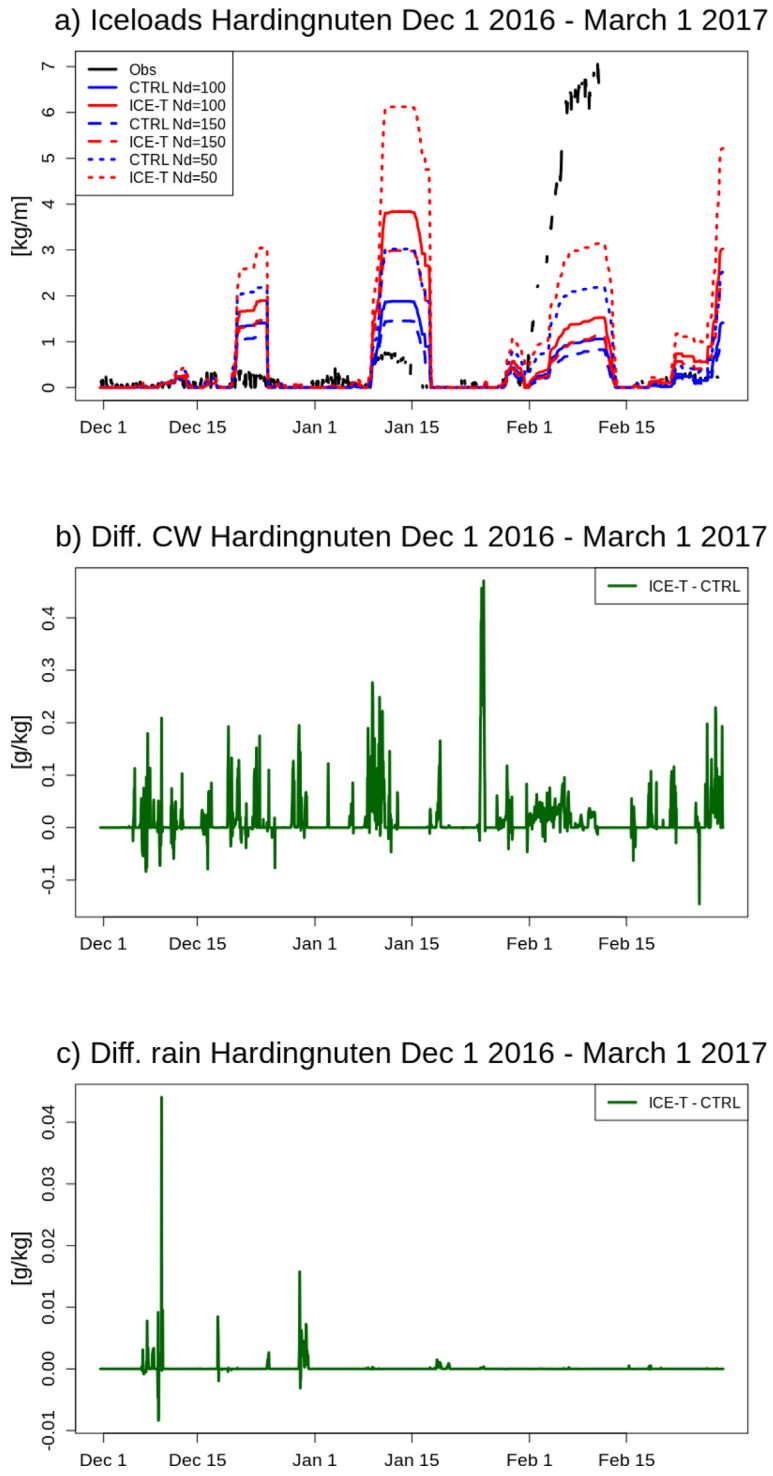

Fig. 8. a) Modelled and observed ice loads at Hardingnuten from Dec 1 2016 to March 1 2017. b) Difference in cloud water mixing ratio (ICE-T - CTRL), and c) difference in rain mixing ratio (ICE-T – CTRL). Date marks represent 1200UTC.

Looking at the difference in distribution (ICE-T - CTRL) in Fig. 6a), a very interesting pattern is revealed. There is a clear tendency of less precipitation at the coastal areas and more precipitation further inland. Yet the total difference in precipitation is small (only 95%).

Separating the precipitation into rain, snow, and graupel reveal the reason for the changed precipitation pattern. There is a pronounced decrease in graupel in ICE-T compared with CTRL (77% of CTRL), especially along the coast line (Fig. 6c). Graupel is increased on the lee side of the mountains, particularly in southern-Norway. The increased graupel in these areas could be due to more available liquid water for riming on snow, or transition from snow into graupel when the melting layer is close to the surface, as snow will first melt into graupel before entering the rain category in our microphysics scheme.

The difference in precipitation in the form of snow shows a similar, yet opposite picture (Fig. 6d). There is a clear increase in snow amounts, 24% more snow in ICE-T, mostly inland. In ENG20 the conditions for snow collecting cloud water were changed, so that the outcome would readily remain in the snow category instead of being

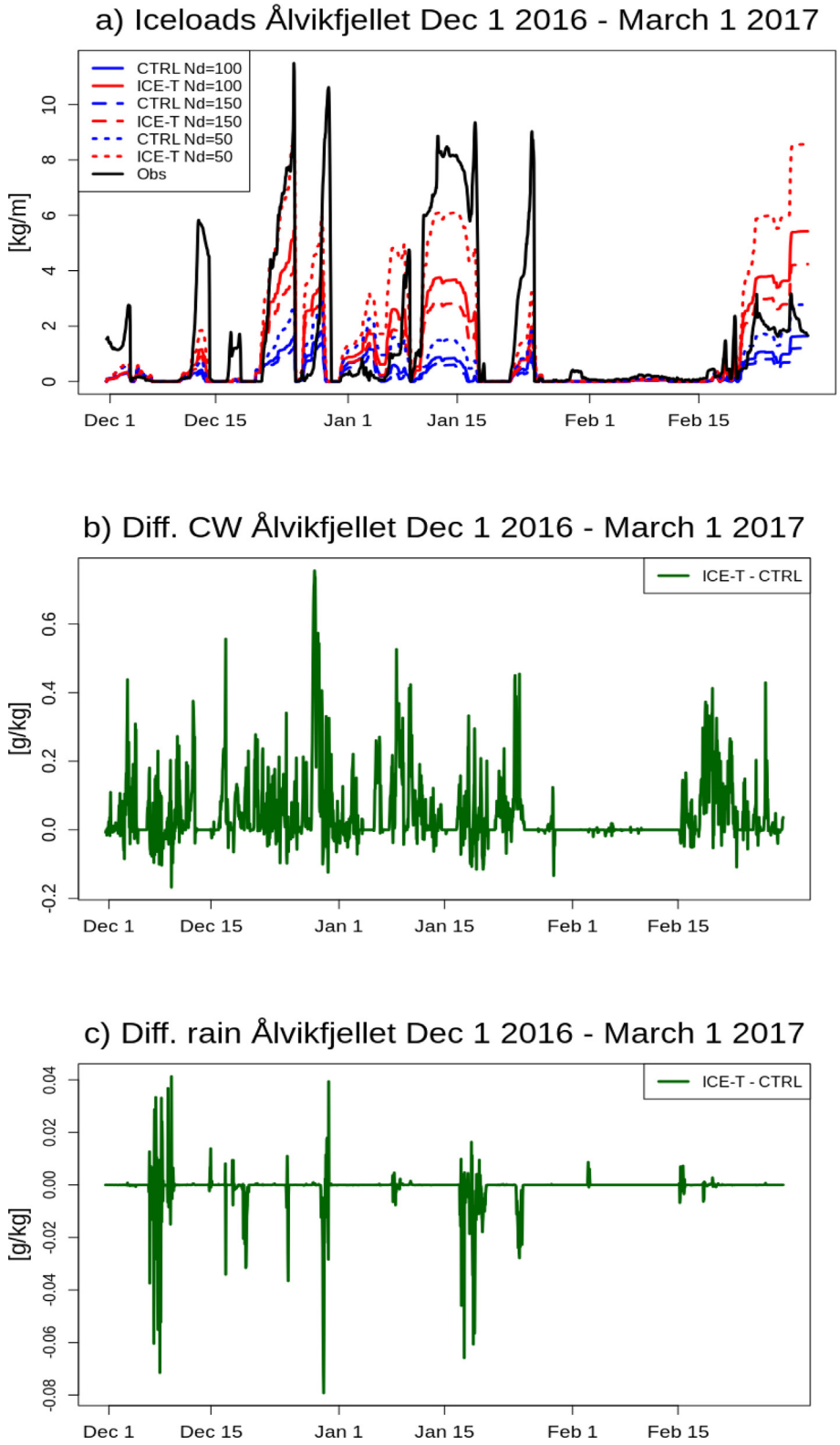

Fig. 9. a) Modelled and observed ice loads at Ålvikfjellet from Dec 1 2016 to March 1 2017. b) Difference in cloud water mixing ratio (ICE-T - CTRL), and c) difference in rain mixing ratio (ICE-T - CTRL).

converted into graupel. The reduction in graupel, and a similar increase in snow, in the ICE-T experiment (compared to CTRL) is likely a consequence of this change. Snow has a lower fall velocity than graupel and will therefore remain longer in the atmosphere, enabling the precipitation to travel further inland, before it reaches the ground.

The difference in rain (Fig. 6e) is small compared with graupel and snow. There is a slight reduction from CTRL (95% of CTRL). We also see the separation between coastal areas and inland, with more rain inland and less along the coast. This can also be explained by the reduction in graupel along the coast and increase in snow inland, as melting graupel

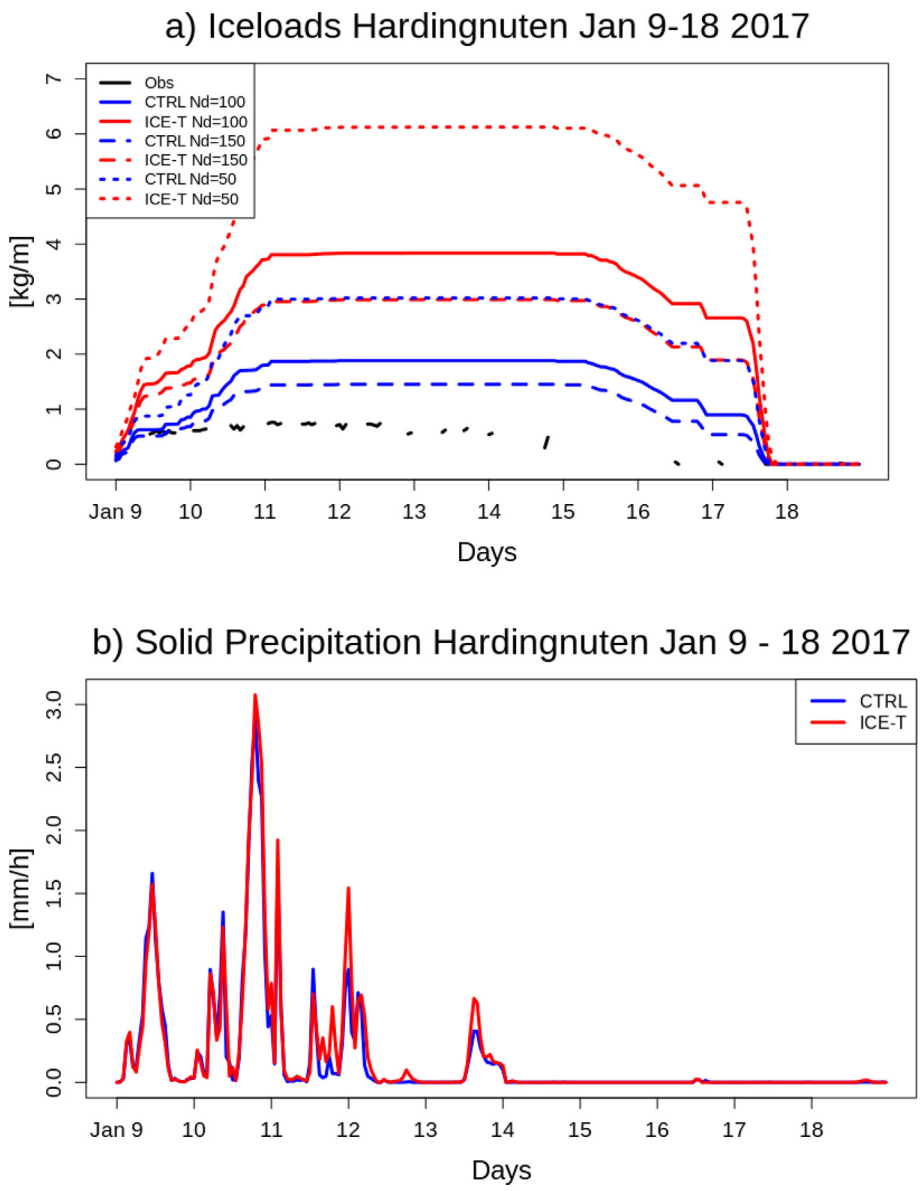

Fig. 10. a) Modelled and observed ice loads at Hardingnuten during case 1. b) Modelled solid precipitation during case 1. Date marks denotes 1300 UTC.

and snow will turn into rain.

In Fig. 5g) and h) there is not much difference in the overall verification of total precipitation. One explanation could be that the coastal areas normally experience a high precipitation rate, so the relative difference in percentage is not very high, around 70–90% of the CTRL precipitation (Fig. 6b). As opposed to the inland areas, where precipitation rates are much lower, the precipitation is increased to 130–150% of the CTRL simulation, with the modified scheme. However, dividing the observation stations into coastal and mountain stations (not shown), did not reveal any large differences in the verification.

Looking at the total accumulated precipitation for all stations, we found that CTRL has a slightly better match with the observed values, than ICE-T. CTRL had too little total precipitation along the coast, and too much in the mountains, a pattern that is enhanced with ICE-T.

When doing the verification with 24 h-precipitation, rather than hourly, we found a larger negative bias for the coastal stations and a larger positive bias for the mountain stations, from CTRL to ICE-T. Standard deviation of error was higher for ICE-T for both mountain and coastal stations.

However, the verification is not just sensitive to the amount of precipitation, but also the timing. By checking the verification of precipitation/no precipitation, ICE-T had more often predicted no precipitation compared with CTRL, which is in better agreement with the observations. To conclude, CTRL has a better spatial distribution of the amount of precipitation, while ICE-T has a better frequency of precipitation/no precipitation.

4.3. Hydrometeor distribution

In addition to the surface precipitation, we also study the vertical distribution of hydrometeors. The values from CTRL are subtracted from ICE-T for each model level, and then integrated over the 35 lowest model levels, which corresponds to an integral approximately between the surface and the 650 hPa level. This covers the lower troposphere where the changes by the microphysics scheme have the most impact. Above this level the changes are small, due to very cold temperatures and little moisture. The results are shown in Fig. 7.

As the aim of the modifications in the cloud microphysics scheme, represented by ICE-T, was to increase the SLW and reduce the amount of cloud ice, we study the partitioning between the hydrometeors to investigate if this holds true in our full 3D weather forecasts. For cloud

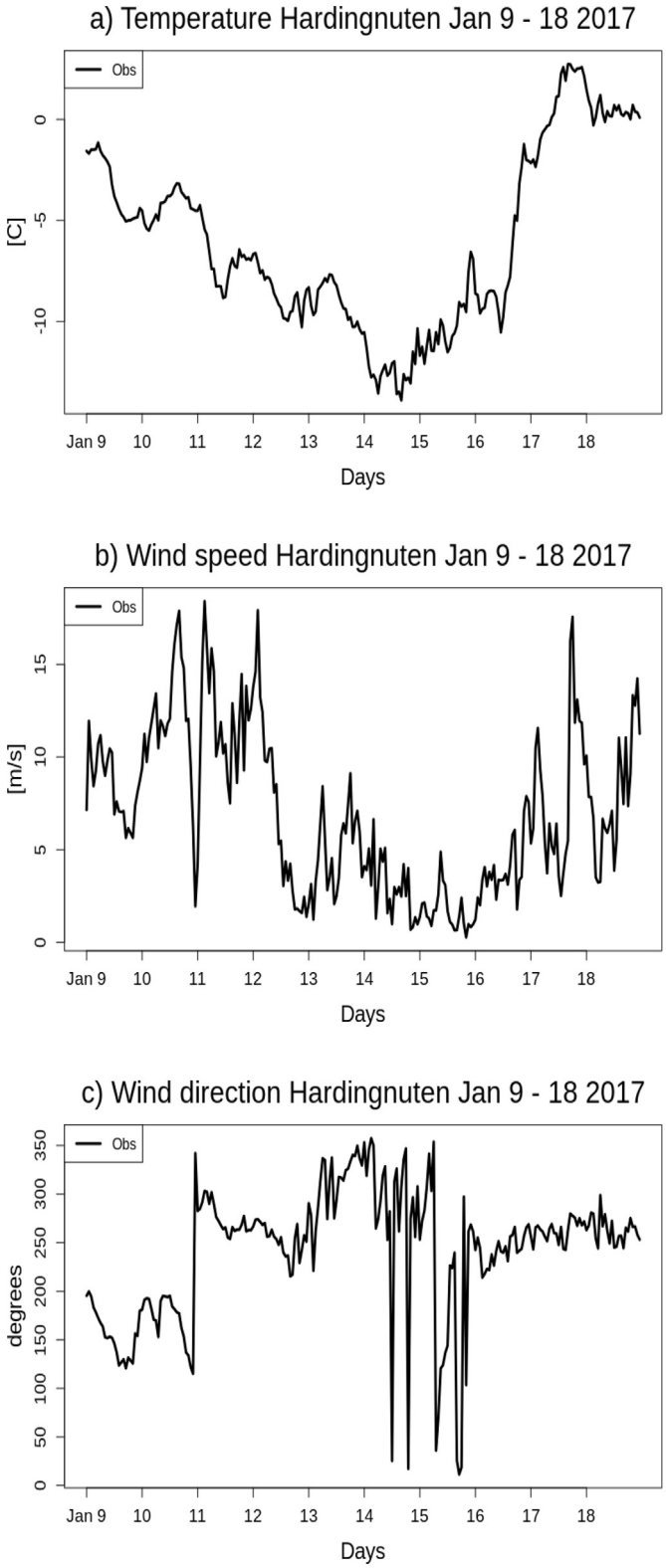

Fig. 11. Observed temperature a), wind speed b), and wind direction c) during case 1 (Jan 9–18 2017). 0° denotes northerly direction for the wind direction. Date marks denotes 1300 UTC.

water (Fig. 7a) there is a clear shift towards higher values in ICE-T compared with CTRL. The changes are most pronounced in south-east Norway, south-western and northern Sweden and northern Finland. Similar to the surface precipitation plot, snow is more abundant in ICE-T with a maximum increase in northern Sweden and Nordland county in Norway (Fig. 7d). There are also some patches of increased vertical distribution of snow in southern Norway and Sweden. The vertical distribution of graupel (Fig. 7c) is generally reduced, yet with some patches of increased graupel, close to the maximum of reduction in graupel in northern Sweden. The difference in cloud ice distribution is much smaller (Fig. 7b), yet also clearly shifted towards lower values in ICE-T, compared with CTRL. There were no clear differences in rain (not shown). Looking only at supercooled cloud water (Fig. 7e), the plot is very similar to cloud water in general, meaning that most of the cloud water is supercooled. There is a clear increase in southeastern Norway and northern Sweden. We can conclude that the changes to the microphysics scheme have increased the amount of SLW in general.

4.4. Ice-loads at Hardingnuten

Next, we use output from the HARMONIE-AROME model to calculate ice-loads following the methodology outlined above. The estimated ice loads for both CTRL and ICE-T, along with the observations, from Dec 1 2016 at 1200UTC to March 1 2017 1100UTC, can be found in Fig. 8. For most of the period, the observed ice loads were quite small, less than 1 kg/m, except for a few days in February, where the peak measured ice loads exceeded 7 kg/m.

The estimated ice loads from the simulations, however, show several peaks of high ice loads in both December and January, and also at the end of the simulation period in late February. In all the modelled icing events, the observations show traces of icing, yet the observed values are much smaller than the modelled ice loads. For instance, the peak in January corresponds to an observed icing event, but maximum ice loads are only 0.76 kg/m, well below the estimated ice loads of 1.89 and 3.88 kg/m for CTRL and ICE-T with Nd = 100, respectively.

For the observed February event, however, the maximum ice loads were measured to 7.05 kg/m, while both CTRL and ICE-T underestimates the ice loads with max ice loads of 1.32 and 1.77 kg/m with Nd = 100, respectively. With a low droplet number concentration set in the ice accretion model (Nd = 50), the maximum estimated ice loads become 2.46 and 3.41 kg/m for CTRL and ICE-T, respectively, which is still far below the observed values.

Overall, the modified microphysics scheme (ICE-T) results in higher estimated ice loads than the original scheme (CTRL). However, the sensitivity to Nd is large. For instance, the mean ice load is 1.15 kg/m for ICE-T with Nd = 50, and 0.49 kg/m for ICE-T with Nd = 150.

By looking at the cloud water mixing ratio for CTRL and ICE-T over the same time period, it is obvious that the overall higher estimated ice loads in ICE-T stems from more liquid cloud water available. In Fig. 8b) the cloud water mixing ratio at Hardingnuten is plotted. Only a few times is the cloud water mixing ratio higher for CTRL, than for ICE-T. There is very little rain present during the entire period, and the difference between CTRL and ICE-T is not that large (Fig. 8c).

Even though ICE-T has higher estimated ice loads, the timing of the events are similar to CTRL. This means that ICE-T is not capable to capture more observed events than the original scheme, but does not increase the false alarm rate either. We can conclude that the presence of cloud water is governed by the larger dynamical factors, and the amount is sensitive to the choice of microphysical parameterisations.

4.5. Ice-loads at Ålvikfjellet

Ålvikfjellet measurement site experienced several icing events during the winter season 2016–2017, with the highest registered values being between 10 and 12 kg/m. Overall, the timing of the observed icing events are quite well captured by the simulations (Fig. 9). Similar to Hardingnuten, the estimated ice loads are higher for ICE-T than CTRL. The modelled values in ICE-T seem to be more in agreement with the observed values for this site, yet the ice loads are generally underestimated. The mean observed values are 1.62 kg/m, while for ICE-T and CTRL with Nd = 100, the corresponding values are 1.12 kg/m and

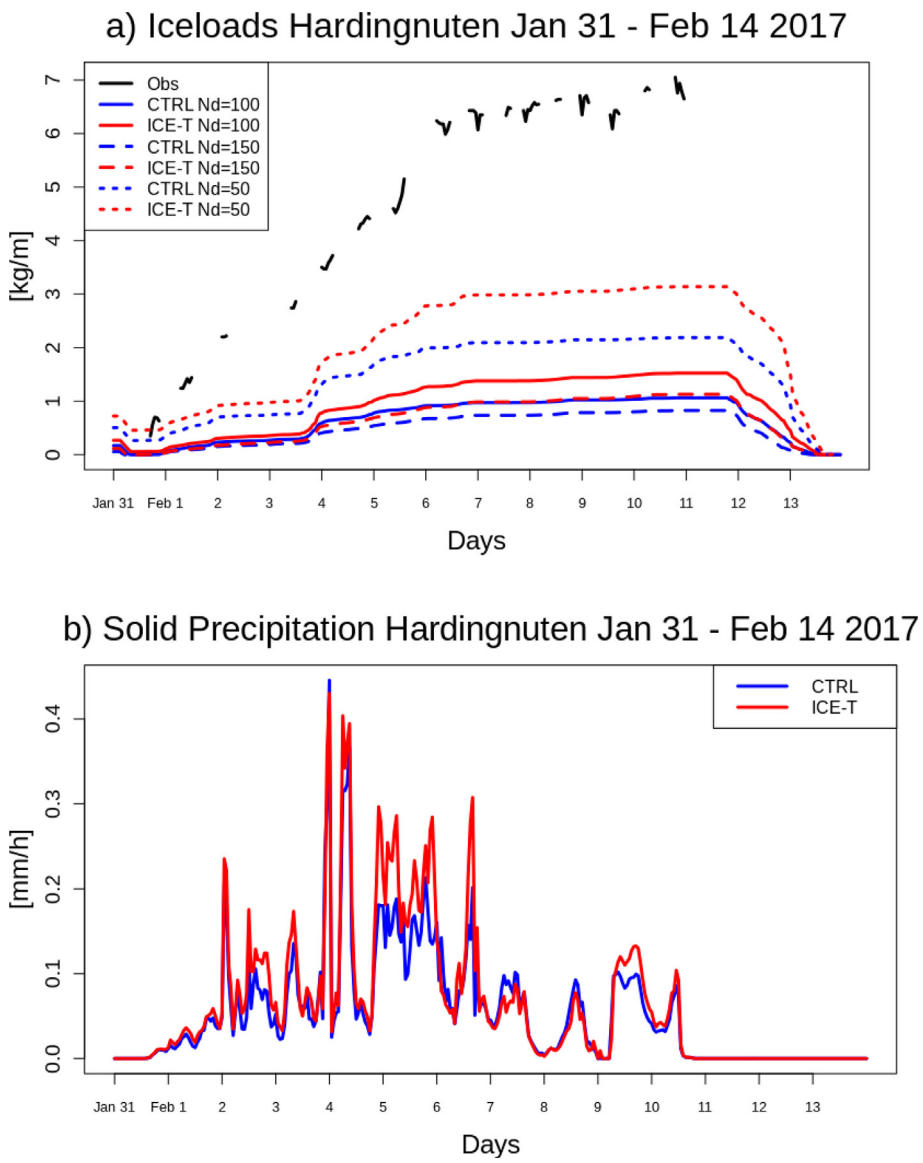

Fig. 12. a) Modelled and observed ice loads at Hardingnuten during case 2. b) Modelled solid precipitation during case 2. Date marks represent 1300 UTC.

0.34 kg/m, respectively.

The long period without any registered icing from late January to mid-February is also well captured by both simulations. As in the Hardingnuten case, the choice of Nd is important. For the icing event Jan 9–18 2017, Nd = 50 gives a maximum ice load of 6.1 kg/m for ICE-T, while the corresponding value is only 2.9 kg/m with Nd = 150. Likewise, the mean ice load for ICE-T is 1.83 kg/m for Nd = 50, and 0.86 kg/m with Nd = 150.

4.6. Cases

To get a better understanding of the results, we dive deeper into a few cases, namely Jan 9–18 and Feb 1–14 2017 at Hardingnuten. In the first case, the models greatly overestimated the ice loads, while in the second case, the models underestimated the ice loads at Hardingnuten. We here investigate why the two time-periods resulted in opposing behaviour.

4.7. Jan 9 - 18 2017

The observed ice loads at Hardingnuten start at approximately zero on Jan 9 2017 (Fig. 10a). The ice load increases up to 0.75 kg/m on Jan 11 and Jan 12. Most of the ice accretion happens during the evening of Jan 9, continuing with small amounts during the morning of Jan 11. The ice load gradually decreases from the morning of Jan 13 until there is no ice left on Jan 16. Since the temperature is below zero the entire period, the ice loss must be due to either sublimation and/or mechanical shedding, however, since the decrease in ice mass is gradual, shedding is unlikely. The temperature varied between −1 to −9 °C (Fig. 11a), with the most ice accretion happening around −5 °C.

The modelled ice loads (using both CTRL and ICE-T NWP model output and Nd = 100) also start at approximately zero on Jan 9, and increases gradually to 1.89 (CTRL) and 3.88 kg/m on Jan 11, much higher than the observed ice loads. Sublimation happens from Jan 15, before everything melts during a few hours on Jan 17.

A possible explanation of the difference in modelled and observed ice loads, is the shielding effect mentioned in the methodology section. The orographic enhancement of the cloud water is somewhat reduced with winds from southwest to southeast due to slightly higher terrain upstream of the measurement station. The model terrain is obviously much smoother and the shielding terrain upstream is not present in the model in the same way as in reality (see Fig. 4a). The observed wind direction is from west/southwest in the morning on Jan 9 (Fig. 11b,c), turning southerly in the afternoon and then southeasterly in the

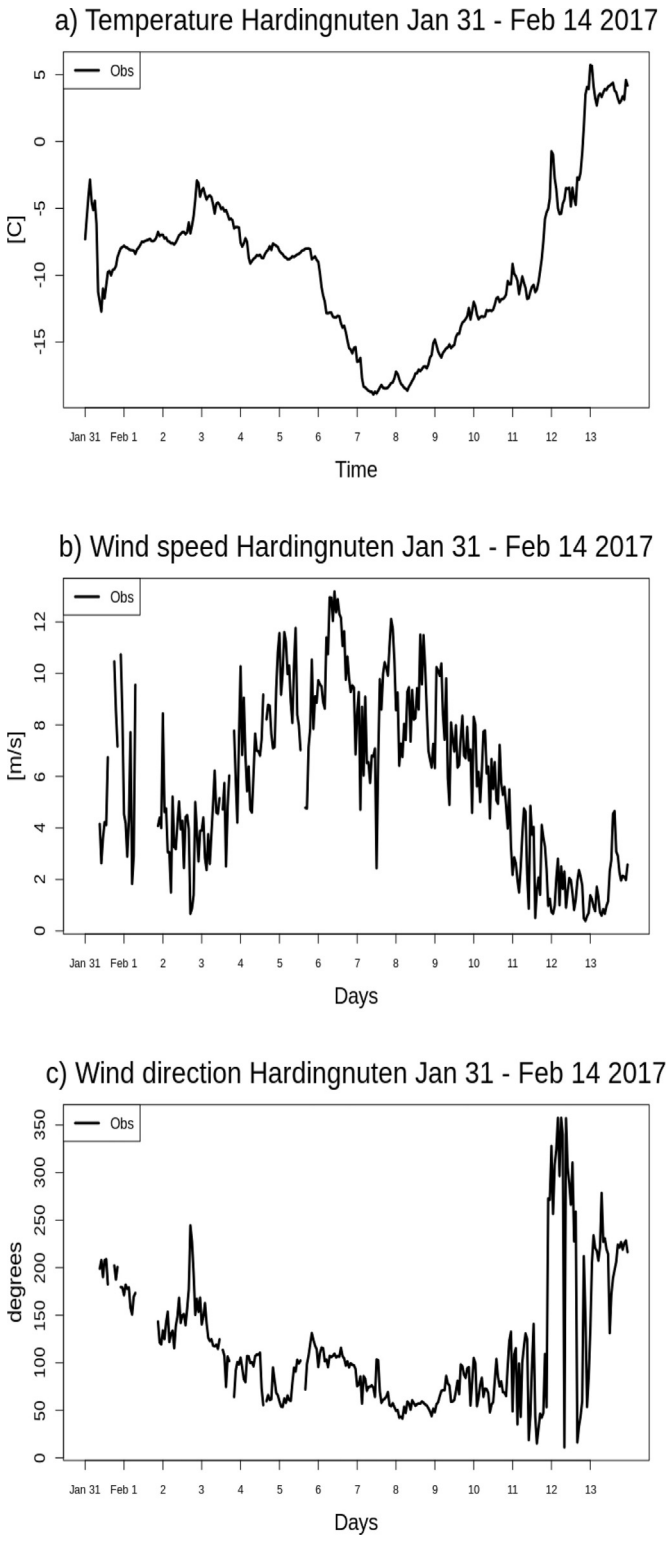

Fig. 13. Observed temperature a), wind speed b), and wind direction c) during case 2 (Jan 31 – Feb 14 2017). 0° denotes northerly direction for the wind direction. Date marks denotes 1300 UTC.

evening. The wind direction remains mostly southerly or southeasterly during the rest of the ice accretion period, until the afternoon of Jan 11, when both the modelled and observed ice accretion had stopped.

Another effect that could explain the overestimated ice loads, is the balance between cloud water and solid precipitation. Cloud water content could be overestimated if the NWP model does not produce snow or graupel according to the observations. There is no precipitation gauge present at the site, however, a web camera was installed to monitor the IceTroll, in addition to a disdrometer mounted on the site. The camera images show fog from the afternoon of Jan 9 and throughout Jan 10 and most of Jan 11. It is hard to see if snow is present, but there appears to be some snow on the images from the morning hours of Jan 10 and also afternoon on Jan 11 (not shown). The disdrometer shows traces of larger particles (not shown), but it is difficult to determine whether or not there is solid precipitation present.

The model simulations have snow between the afternoons of Jan 10 and Jan 11 (Fig. 10b), approximately when the modelled ice accretion is most active. It is therefore unlikely that underestimated solid precipitation - leading to an overestimation of suspended cloud water could thus have contributed to the overestimation of the ice accretion.

4.8. Feb 1 - 14 2017

During this period, the situation is the opposite of the previous case. Here, the modelled ice loads were much lower than the observed values. It is a unique case because most of the ice accretion is registered when the temperatures are below −8 °C and even down to −13 °C (Fig. 13a). At these low temperatures most NWP models will have converted most of the liquid water to ice, so this case is a real challenge to model.

Ice loads of approximately 0.5 kg/m are detected at Hardingnuten already on Feb 1 (Fig. 12a). It is difficult to place the onset of the ice accretion, as some observations are missing. The ice loads gradually increase until Feb 7 (approx. 6.5 kg/m), and then again on Feb 10 and 11 when a maximum value is reached at 7.05 kg/m. This is followed by a period of missing values, before most of the ice is gone on Feb 15. From Feb 13, the temperature increases above 0 °C, so it is likely melting that removes the ice. This is further supported by camera images at the site (not shown).

Both simulations give a starting value of ice loads of approximately 0 kg/m with Nd = 100 on Feb 1. This gradually increases to 1 kg/m (CTRL) and 1.4 kg/m (ICE-T) on Feb 7. Then the ice loads continue to grow from Feb 10, until the maximum values of 1.06 kg/m (CTRL) and 1.52 kg/m (ICE-T) are reached on Feb 11. There is a good correlation between modelled and observed timing of ice accretion, although the values are too low. With Nd = 50, the maximum modelled ice loads increase to 2.19 kg/m and 3.14 kg/m for CTRL and ICE-T, respectively. Definitely an improvement, yet still too low compared with the observations.

There are a number of possible reasons for the underprediction of the ice loads in this case. This is a cold case, with icing in temperatures around −10 °C, which is difficult for NWP models, as they often have a tendency to produce ice at the expense of liquid water. Similar to the Jan 9–18 case, the balance between supercooled liquid and snow in the simulations could differ from reality. Fig. 12b) shows that there is little solid precipitation present in the model simulations during the period. The camera images show mostly foggy conditions until Feb 7. Snowfall can be seen during the morning hours of Feb 10 (not shown), and possibly in the afternoon of Feb 5 and 6. The disdrometer data show traces of solid precipitation on Feb 5, 9, and 10 (Fig. 14), but lacks data from Feb 6–8. It is hard to estimate what the correct amount of precipitation should be, yet with so low values in the model simulations, it is unlikely that the model suppresses generation of SLW due to excessive production of snow and graupel.

The wind is mostly from the east during the heaviest icing periods (Fig. 13b,c). It is occasionally from southeast, but not long enough to give much shielding. It is likely that in this case the observation site at Hardingnuten did not experience much shielding from the terrain upstream, leading to higher observed ice loads than in the first case. Instead, the narrow valley to the north-east of the site could have contributed to an enhancement of the supercooled liquid water, due to the lifting of air masses from around 200–300 to 1200 m.a.s.l. in the actual

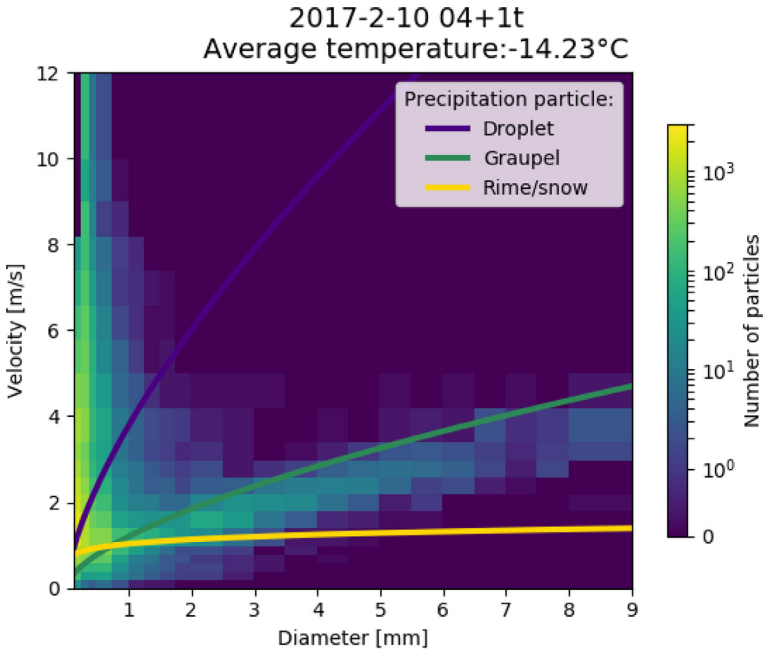

Fig. 14. Disdrometer data from Feb 10 at 0400UTC.

terrain (see Fig. 4b). This valley is poorly resolved by the model, and the corresponding lift is only from 700 to 1100 m.a.s.l.

The modelled ice loads are also very sensitive to the cloud droplet number concentration, and it is difficult to know the exact value of Nd. It could be argued that even a number concentration of 50/cm^3 -is too high, or 150/cm^3 is too low in some cases. The large-scale wind direction could also influence Nd, as the air masses could vary from relatively clean air from unpolluted areas, to air transported from cities and industrial areas.

5. Discussion and conclusions

The key question that we are addressing in this study is if an improved representation of supercooled liquid water in numerical weather prediction can lead to better predictions of atmospheric icing. While the comparison between observed and modelled ice-loads is an immensely challenging task - impacted by synoptic scale flow patterns, terrain, microphysical processes, and ice build-up on the instruments themselves - our findings suggest that the modified microphysics scheme, through an improved representation of SLW, improve the magnitude of modelled ice-loads.

Overall, we found higher amounts of cloud water with the new microphysics scheme, ICE-T, compared with CTRL, and most of this cloud water was supercooled. This was evident both in the column integrated values over the entire domain and also in the time series from the two observation stations Hardingnuten and Ålvikfjellet. Our findings also indicated a clear change towards less cloud ice, more snow, and less graupel. For the surface precipitation, ICE-T had 77% of CTRL's graupel, and 124% of the snow. This was traced back to the change in snow collecting cloud water (SCW) from changes in the microphysics scheme, presented in ENG20, where the resulting hydrometeor would more often remain snow, rather than change into graupel. The total precipitation amount was slightly reduced, 95% of CTRL, yet the geographical distribution has changed to less precipitation along the coast and more precipitation inland. We hypothesise that this is an effect of the switch to more snow and less graupel, as snow has lower fall speed and follow the airflow further inland before it precipitate out. Since we do not separate between graupel and snow in the observations, it is hard to verify if the change has lead to an improvement or not.

Even though the spatial distribution of the amount of precipitation is somewhat degraded with ICE-T, we believe that the modifications in ICE-T leading to more snow and less graupel are physically better than CTRL, and that there are compensating errors in the HARMONIE-AROME physics that could be responsible for the precipitation bias. For instance, the cloud condensation nuclei (CCN) is set to 100 /cm^3 over sea and 300 /cm^3 over land. This sharp transition will lead to smaller droplets along the coast line, than we would expect with relatively clean maritime air, and suppress precipitation through reduced autoconversion and snow/graupel collecting cloud water. Preliminary runs with variable CCN show an improvement in the precipitation bias.

Specifically, the results showed an overall better agreement with the observed ice loads using ICE-T compared with CTRL microphysics for the predicted ice loads at Ålvikfjellet. The observed values were generally higher than the modelled values, so with the higher amounts of cloud water, the estimated ice loads were naturally higher with ICE-T. The results at Hardingnuten are more difficult to interpret. For some cases both simulations overestimates the ice loads, while in the February case, ice loads are underestimated by both simulations. The overestimation around Jan 9–18 is most likely a result of shielding by the terrain from icing from the southeast, that is not captured by the model terrain. While the February case could have experienced enhanced SLW due to lifting of the air masses coming from the east. Higher resolution could improve the estimated ice loads (Nygaard et al., 2011).

Another explanation for the underestimation (overestimation) of cloud water is the overproduction (underproduction) of snow and graupel at the expense of liquid water. After checking the camera images and disdrometer data from the Hardingnuten site, this does not appear to be valid for either cases. It is likely the low temperatures observed during the Feb 1–14 case lead to the underestimation of the ice loads by the simulations. ICE-T leads to more supercooled cloud water, however, perhaps not enough during very cold temperatures.

Even though the modified microphysics scheme resulted in higher estimated ice loads, the timing of the modelled icing events did not change. However, it appears that the timing of the events were quite well predicted in the first place, suggesting that the atmospheric icing is governed mostly by larger dynamical effects, and not so much by the microphysics in itself.

It is difficult to use observed ice loads as a proxy for SLW. A large

uncertainty in the estimation of the ice loads is the sensitivity to the cloud droplet number concentration (Nd). This is hard to quantify and the results show huge variations within the range of Nd = 50 to Nd = 150 particles per cm^3. An accurate description of the number concentration is important also for the microphysics schemes in HARMONIE-AROME themselves. The cloud droplet number concentration impacts the droplet sizes, which in turn impact microphysical processes, and subsequently the liquid water content output from the NWP model. Thompson et al. (2017) argues that the cloud droplet number concentration is likely to vary from 25 to 1000/cm^3 over the entire US continent, and Hines and Bromwich (2017) argued that it could be as low as 1/cm^3 in arctic regions, which would actually inhibit cloud formation. A better estimate of the cloud droplet number concentration is therefore needed for more accurate ice loads as well as precipitation and cloud cover forecasts.

Taking the challenges with sub-grid terrain effects at Hardingnuten into account, most of the icing events were underpredicted by the simulations. ICE-T gives the highest values of SLW and therefore also the most accurate estimates of the ice loads during the winter season of 2016–2017.

In an upcoming study, we will focus on ICE-T's ability to forecast icing for aviation purposes. We will study cases of reported icing on aircraft, and study the vertical distribution of SLW, especially changes in vertical levels where SLW is present between CTRL and ICE-T. We will also use satellite data to verify the ice and liquid water content of the clouds. Together with the current study, this will give a comprehensive verification of ICE-T's representation of SLW.

Declaration of Competing Interest

The authors declare that they have no known competing financial interests or personal relationships that could have appeared to influence the work reported in this paper.

Acknowledgements

We would like to thank Trude Storelvmo at the University of Oslo and Mareile Wolff from MET-Norway for valuable discussions and comments. We would also like to thank Morten Køltzow and Teresa Valkonen at MET-Norway for valuable input on the simulation setup. Thanks to Rolv Bredesen at Norconsult for nice figures of cross section of model and actual terrain. Parts of this study have been published as a conference proceeding: Engdahl et al. (2019) for the IWAIS 2019 conference. This work is a part of the WISLINE project funded by the Norwegian Research Council, grant 244106/E10. Lastly, we would like to dedicate this work to the late Professor Jón-Egill Kristjánsson whom suffered a tragic accident after initiating this study. Professor Kristjánsson was an advocate for basic research, but was also keen to emphasise that the results should be used for the public good and often collaborated with the operational weather service in Norway, this study is an example of the legacy he left behind.

References

Atlas, David, Ulbrich, C.W., 1977. Path- and Area-Integrated Rainfall Measurement by Microwave Attenuation in the 1–3 cm Band. Journal of Applied Meteorology. American Meteorological Society 16 (12), 1322–1331.

Belo-Pereira, M., 2015. 'Comparison of in-Flight Aircraft Icing Algorithms Based on ECMWF Forecasts', *Meteorological Applications*. Wiley Online Libraryhttps://doi.org/10.1002/met.1505. Available at:.

Bengtsson, L., et al., 2017. The HARMONIE–AROME Model Configuration in the ALADIN–HIRLAM NWP System'. *Monthly Weather Review*. American Meteorological Society 145 (5), 1919–1935. https://doi.org/10.1175/MWR-D-16-0417.1.

Brousseau, P., et al., 2016. Improvement of the forecast of convective activity from the AROME-France system. Quarterly Journal of the Royal Meteorological Society. Wiley Online Library 142 (699), 2231–2243. Available at. https://doi.org/10.1002/qj.2822.

Cohard, J.-M., Pinty, J.-P., 2000a. A comprehensive two-moment warm microphysical bulk scheme. I: Description and tests. *Quarterly Journal of the Royal Meteorological Society*. Wiley Online Library 126 (566), 1815–1842. Available at. https://doi.org/10.1002/qj.49712656613.

Cohard, J.-M., Pinty, J.-P., 2000b. A comprehensive two-moment warm microphysical bulk scheme. II: 2D experiments with a non-hydrostatic model. *Quarterly Journal of the Royal Meteorological Society*. Wiley Online Library 126 (566), 1843–1859. Available at. https://doi.org/10.1002/qj.49712656614.

Engdahl, B.J.K., et al., 2019. Improved Predictions of Atmospheric Icing at MET-Norway. Available at. https://iwais2019.is/images/Papers/059_iwais_cp_BJKE.pdf.

Engdahl, B.J.K., Thompson, G., Bengtsson, L., 2020. Improving the representation of supercooled liquid water in the HARMONIE-AROME weather forecast model. Tellus. Series A, Dynamic Meteorology and Oceanography. Taylor & Francis 72 (1), 1–18. https://doi.org/10.1080/16000870.2019.1697603.

Farzaneh, M., 2008. Atmospheric Icing of Power Networks. Springer Science & Business Media Available at: https://play.google.com/store/books/details?id=Ufg-AAAAQBAJ.

Ferrier, B.S., 1994. A Double-Moment Multiple-Phase Four-Class Bulk Ice Scheme. Part I: Description. Journal of the Atmospheric Sciences. American Meteorological Society 51 (2), 249–280.

Frogner, I.-L., et al., 2019. 'HarmonEPS - the HARMONIE Ensemble Prediction System', *Weather and Forecasting*. American Meteorological Societyhttps://doi.org/10.1175/WAF-D-19-0030.1.

Hämäläinen, K., Niemelä, S., 2017. Production of a numerical icing atlas for Finland. *Wind Energy*. Wiley Online Library 20 (1), 171–189. Available at. https://doi.org/10.1002/we.1998.

Harstveit, K., Byrkjedal, Ø., Berge, E., 2009. 'Validation of Regional in-Cloud Icing Maps in Norway', in *13th International Workshop on Atmospheric Icing of Structures*. Available at: https://www.compusult.com/html/IWAIS_Proceedings/IWAIS_2009/Session_6_poster/COST%20Action%20727%20WG1/poster_harstveit1.pdf.

Hines, K.M., Bromwich, D.H., 2017. Simulation of Late Summer Arctic Clouds during ASCOS with Polar WRF. Monthly Weather Review. American Meteorological Society 145 (2), 521–541. https://doi.org/10.1175/MWR-D-16-0079.1.

Ingvaldsen, K., et al., 2019. Validation of Modelled in-Cloud Ice Accretion on Overhead Power Lines at Exposed High Altitude Sites in Norway. Available at: https://iwais2019.is/images/Papers/061_IWAIS2019_Ingvaldsen_et_al_Validation.pdf.

Ishizaka, M., 1995. Measurement of falling velocity of rimed snowflakes. *Journal of the Japanese Society of Snow and Ice*. The Japanese Society of Snow and Ice 57 (3), 229–238. Available at. https://www.jstage.jst.go.jp/article/seppyo1941/57/3/57_3_229/_article/-char/ja/.

Kalinka, F., et al., 2017. The In-flight icing warning system ADWICE for European airspace-Current structure, recent improvements and verification results. Meteorologische Zeitschrift *26* (*4*) Stuttgart: Gebrueder Borntraeger Verlagsbuchhandlung, 26(4), pp. 441–455. Available at. https://www.repo.uni-hannover.de/handle/123456789/2632.

Lenderink, G., Holtslag, A.A.M., 2004. An updated length-scale formulation for turbulent mixing in clear and cloudy boundary layers. Q. J. R. Meteorol. Soc. 3405–3427. https://doi.org/10.1256/qj.03.117.

Lin, Y.-L., Farley, R.D., Orville, H.D., 1983. Bulk Parameterization of the Snow Field in a Cloud Model. Journal of Climate and Applied Meteorology. American Meteorological Society 22 (6), 1065–1092.

Liu, C., et al., 2011. High-Resolution Simulations of Wintertime Precipitation in the Colorado Headwaters Region: Sensitivity to Physics Parameterizations. *Monthly Weather Review*. American Meteorological Society 139 (11), 3533–3553. https://doi.org/10.1175/MWR-D-11-00009.1.

Locatelli, J.D., Hobbs, P.V., 1974. Fall speeds and masses of solid precipitation particles. J. Geophys. Res. 79 (15), 2185–2197. https://doi.org/10.1029/JC079i015p02185.

Makkonen, L., 2000. Models for the growth of rime, glaze, icicles and wet snow on structures. *Philosophical Transactions of the Royal Society of London. Series A: Mathematical, Physical and Engineering Sciences*. The Royal Society 358 (1776), 2913–2939. Available at. https://doi.org/10.1098/rsta.2000.0690.

Meyers, M.P., DeMott, P.J., Cotton, W.R., 1992. New Primary Ice-Nucleation Parameterizations in an Explicit Cloud Model. Journal of Applied Meteorology. American Meteorological Society 31 (7), 708–721.

Müller, M., et al., 2017. AROME-MetCoOp: A Nordic Convective-Scale Operational Weather Prediction Model. *Weather and Forecasting*. American Meteorological Society 32 (2), 609–627. https://doi.org/10.1175/WAF-D-16-0099.1.

Neggers, R.A.J., Köhler, M., Beljaars, A.C.M., 2009. A dual Mass Flux Framework for Boundary Layer Convection. Part I: Transport. Journal of the Atmospheric Sciences. American Meteorological Society 66 (6), 1465–1487. https://doi.org/10.1175/2008JAS2635.1.

Nygaard, B.E.K., Kristjánsson, J.E., Makkonen, L., 2011. Prediction of In-Cloud Icing Conditions at Ground Level using the WRF Model. Journal of Applied Meteorology and Climatology. American Meteorological Society 50 (12), 2445–2459. https://doi.org/10.1175/JAMC-D-11-054.1.

Nygaard, B.E., et al., 2017. Development of a reliable modelling system for the calculation of rime ice loads on overhead transmission lines. Proc. IWAIS.

Rutledge, S.A., Hobbs, P.V., 1984. The mesoscale and microscale structure and organization of clouds and precipitation in midlatitude cyclones. XII: a diagnostic modeling study of precipitation development in narrow cold-frontal rainbands. J. Atmos. Sci. 41 (20), 2949–2972. Available at. https://doi.org/10.1175/1520-0469(1984)041%3C2949:TMAMSA%3E2.0.CO;2.

Seity, Y., et al., 2011. The AROME-France Convective-Scale Operational Model. Monthly Weather Review. American Meteorological Society 139 (3), 976–991. https://doi.org/10.1175/2010MWR3425.1.

Tan, I., Storelvmo, T., Zelinka, M.D., 2016. Observational constraints on mixed-phase clouds imply higher climate sensitivity. Science 352 (6282), 224–227. https://doi.org/10.1126/science.aad5300.

Termonia, P., Fischer, C., Bazile, E., Bouyssel, F., Brozková, R., et al., 2018. The ALADIN System and its canonical model configurations AROME CY41T1 and ALARO CY40T1. Geosci. Model Dev. 11 (1), 257–281. Available at: https://www.geosci-model-dev.net/11/257/2018/.

Thompson, G., Rasmussen, R.M., Manning, K., 2004. Explicit Forecasts of Winter Precipitation Using an Improved Bulk Microphysics Scheme. Part I: Description and Sensitivity Analysis. Monthly Weather Review. American Meteorological Society 132 (2), 519–542.

Thompson, G., et al., 2008. Explicit forecasts of Winter Precipitation using an improved Bulk Microphysics Scheme. Part II: Implementation of a New Snow Parameterization. Monthly Weather Review. American Meteorological Society 136 (12), 5095–5115. https://doi.org/10.1175/2008MWR2387.1.

Thompson, G., Politovich, M.K., Rasmussen, R.M., 2017. A numerical weather model's ability to predict characteristics of aircraft icing environments. Weather Forecast. 32 (1), 207–221. Available at. https://doi.org/10.1175/WAF-D-16-0125.1.